EUROPEAN LABORATORY FOR PARTICLE PHYSICS

**Divisional Report**

**CERN/TIS-RP/95-20/PP**
**1/10/96**

# Double differential distributions and attenuation in concrete for neutrons produced by 100-400 MeV protons on iron and tissue targets

S. Agosteo[1], A. Fassò[2], A. Ferrari[3], P.R. Sala[3], M. Silari[4] and P. Tabarelli de Fatis[5]

(1) Politecnico di Milano, Dipartimento di Ingegneria Nucleare, Via Ponzio 34/3, 20133 Milano, Italy
(2) CERN, 1211 Geneve 23, Switzerland
(3) Istituto Nazionale di Fisica Nucleare, Sezione di Milano, Via Celoria 16, 20133 Milano, Italy
(4) Consiglio Nazionale delle Ricerche, Istituto Tecnologie Biomediche Avanzate, Via Ampère 56, 20131 Milano, Italy
(5) Fondazione TERA, Via Puccini 11, 28100 Novara, Italy



## ABSTRACT

Double differential distributions of neutrons produced by 100, 150, 200, 250 and 400 MeV protons stopped in thick iron and soft tissue targets were calculated by two Monte Carlo codes, FLUKA and LCS, from 0° (forward shielding) to 180°. The results are compared with calculated and experimental data available in the literature. The attenuation in ordinary concrete of the dose equivalent due to neutrons and other particles was calculated. The contribution due to photons and protons was found to range from a few percent up to 50 % of the total dose equivalent. Source terms and attenuation lengths are given as a function of energy and emission angle.

*Extended version of paper presented at the*
*2nd Specialists' Meeting on*
*Shielding Aspects of Accelerators, Targets and Irradiation Facilities,*
*CERN, Geneva, Switzerland, 19-23 October 1995*

## Introduction

Proton accelerators in the intermediate energy range (a few hundred MeV), mainly used in nuclear physics until a few years ago, are now finding an increasing number of applications in radiation therapy of cancer, in industry and in various domains of research. A number of facilities are being built or planned worldwide [1-4]. Machines in this energy range are also employed as injectors to accelerators of energy in the GeV region and above.

Shielding of these accelerators requires particular attention, either due to the high intensities required for industrial or research applications or, in the case of radiation therapy, because they need to be installed in a hospital environment and are often located in highly populated areas. The radiation field dictating the shielding requirements is mainly due to secondary neutrons produced by the interaction of the proton beam with the structures of the accelerator and with the beam transfer lines. In the case of medical machines, protons also interact with the beam delivery system used to irradiate the patient (such as collimators), and with the patient himself (where the remaining beam is ultimately lost).

Shielding data in this energy range are not abundant in the literature and are usually limited to specific conditions, geometries and energy values [5]. To overcome this lack of information, the attenuation through ordinary concrete of the dose equivalent produced by 100, 150, 200, 250 and 400 MeV protons stopped in thick iron and soft tissue targets were calculated by two Monte Carlo codes, FLUKA and LCS, from 0° (forward shielding) to 180°. Backward angles were included to account for special conditions found in modern radiation therapy facilities, where the beam extracted from the accelerator can be rotated 360° around the patient by means of a large mechanical structure (isocentric gantry). The iron target reproduces the structural materials of the accelerator and beam transfer lines (mainly the magnets), while tissue represents the patient. The results of the calculations were fitted by the classical two-parameter formula. The source terms and attenuation lengths derived as a function of proton energy and emission angle can be used to design shielding of proton accelerators in any realistic geometry. The results are compared with calculated and experimental data available in the literature. As a first application, the present data were employed in the shielding design of hospital-based proton radiation therapy facilities [6]. The calculated dose equivalent behind the shield includes contribution from both neutrons and their secondaries produced in the concrete. The complete numerical data can be found in the Appendix.

**Neutron source: energy and angular distributions**

The energy and angular distributions of neutrons produced by a monoenergetic and monodirectional proton beam ("pencil beam") impinging on an iron or soft tissue target, were calculated by the LCS [7] and FLUKA [8] Monte Carlo codes. The target is cylindrical, with the axis coincident with the incoming beam direction, and is slightly thicker than the proton range in the material at the given energy. For soft tissue, the elemental composition of ICRU 33 [9] has been adopted. A comparison of double differential distributions predicted by FLUKA at a proton energy of 256 MeV with experimental data [10] is shown in Fig. 1. A comparison of the same experimental data with LCS results has already been published by Prael et al. [11]. The two codes agree better in the forward direction than at large angles (Fig. 2). This is probably due to the lack of the pre-equilibrium module in the LCS version used.

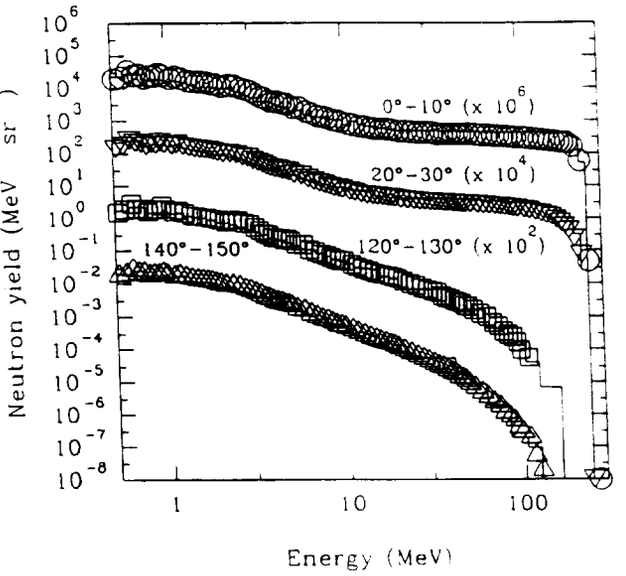


Fig. 1 Comparison between FLUKA double differential neutron distributions per proton and experimental data for 256 MeV protons striking a thick iron target. O 7.5°, ▽ 30°, □ 130°, △ 150°.

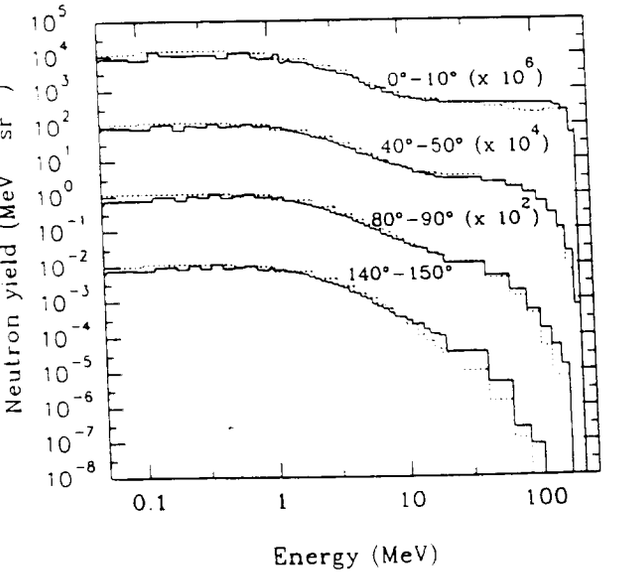


Fig. 2 Comparison between FLUKA and LCS double differential neutron distributions per proton for 200 MEV protons striking a thick iron target. Solid lines FLUKA, dashed lines LCS.

A preliminary set of simulations was also carried out to assess the target radius which would ensure the most conservative combination between neutron yield and spectrum hardness (Fig. 3). As a general rule, the larger the transverse dimension of the target, the higher is the yield and the lower is the average energy of the distribution. Differences at low energy are of no relevance for shielding. As the high energy neutron yield varies little with target size, the radius of the target was chosen according to practical considerations (e.g., typical dimensions of machine components). Table 1 lists the target parameters used in the calculations.

Figs. 4-13 show the double differential distributions produced by 100-400 MeV protons on iron and soft tissue, calculated with FLUKA. The statistical errors associated to the distributions are below 15 % in the angular interval 0°-90° and below 40 % in the interval 90°-180°. Table 2 lists the integrated neutron yields as calculated with FLUKA (100-400 MeV).

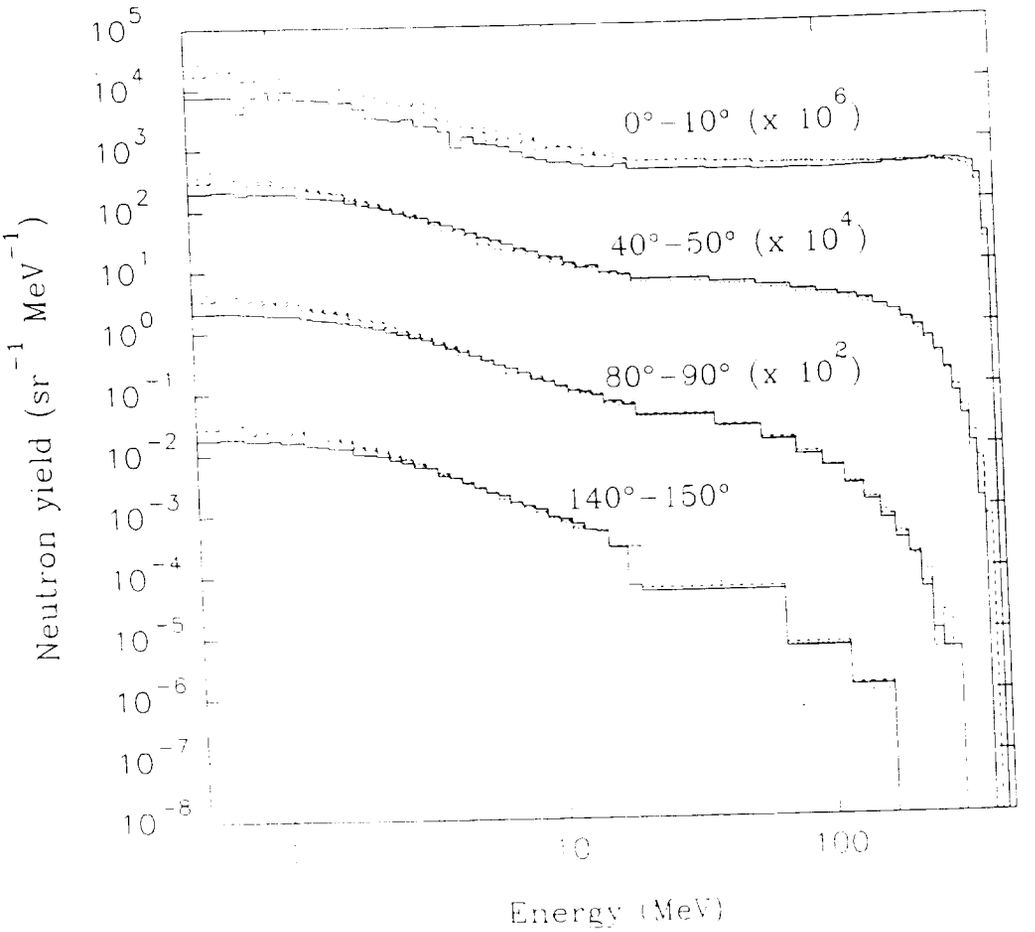


Fig. 3 Comparison between double differential neutron distributions per proton for 400 MeV protons striking thick iron targets of different radii. Solid lines show neutron distributions from a target of 1 cm radius, long dashed lines 3 cm radius, medium dashed lines 5 cm radius and short dashed lines 7.5 cm radius.

**Table 1** Target dimensions used in the Monte Carlo simulations.

| | Iron ρ=7.87 g cm$^{-3}$ | | | Tissue ρ=1.0 g cm$^{-3}$ | | |
|---|---|---|---|---|---|---|
| $E_p$ (MeV) | Range (mm) [ref. 12] | Radius (mm) | Thickness (mm) | Range (mm) [ref. 12] | Radius (mm) | Thickness (mm) |
| 100 | 14.45 | 10 | 20 | 75.78 | 40 | 80 |
| 150 | 29.17 | 15 | 30 | 155.1 | 85 | 170 |
| 200 | 47.65 | 25 | 50 | 255.4 | 135 | 270 |
| 250 | 69.30 | 58 | 75 | 373.5 | 210 | 420 |
| 400 | 149.05 | 75 | 150 | 810.8 | 210 | 820 |

**Table 2** Thick target neutron yield.

| | Yield (neutron per incident proton) | | | |
|---|---|---|---|---|
| $E_p$ (MeV) | Iron n <20 MeV | $n_{tot}$ | Tissue n <20 MeV | $n_{tot}$ |
| 100 | 0.0337 | 0.1094 | 0.0104 | 0.1024 |
| 150 | 0.0602 | 0.2079 | 0.0154 | 0.1383 |
| 200 | 0.0980 | 0.4400 | 0.0181 | 0.3011 |
| 250 | 0.1590 | 0.7687 | 0.0202 | 0.5154 |
| 400 | 0.3360 | 2.5061 | 0.0279 | 1.7409 |

**Neutron attenuation in concrete**

The neutron production and attenuation in ordinary concrete (type TSF 5.5, Table 3) were computed with FLUKA for slab thicknesses from 0 to 600 cm and with LCS for thicknesses from 0 to 180 cm. Variance reduction techniques are not available in the LCS code above 20 MeV; calculations for larger shield thicknesses were therefore not performed because of insufficient statistics. The results obtained with the two codes for slab thicknesses up to 180 cm and 90° are in agreement, in spite of the differences in the emission at large angles.

**Table 3** Elemental composition, percent water content and density of concrete TSF-5.5.

| Elemental composition ($10^{21}$ atoms cm$^{-3}$) | | | | | | | | Water content (by weight) | density (g cm$^{-3}$) |
|---|---|---|---|---|---|---|---|---|---|
| H | C | O | Mg | Al | Si | Ca | Fe | | |
| 8.50 | 20.20 | 35.50 | 1.86 | 0.60 | 1.70 | 11.30 | 0.19 | 5.5% | 2.31 |

Monte Carlo calculations were made from 0° to 180° with FLUKA and from 0° to 90° with LCS, both in spherical and slab geometries. The inner radius of the sphere was sufficiently large to ensure that effects related to curvature are negligible. Results obtained in the two geometries agree within the statistical errors (Fig. 14). The source was located in the centre of the target. The dose equivalent due to the neutrons transmitted through the shield was calculated by folding the fluence with appropriate fluence to ambient dose equivalent conversion factors. Since up-to-date conversion factors for neutrons up to 400 MeV, "officially" recommended, are not yet available, three sets of coefficients in common use were employed [13-15]. Conversion factors for photons were taken from ref. [16].

Amongst the variance reduction techniques available in FLUKA, use was made of "geometry splitting" and "russian roulette", adjusting the importances so as to maintain the number of particles approximately constant with increasing concrete thickness. Each data point is the average of the results of a number of independent simulations. The total number of protons per data point was at least 500'000 with FLUKA and 200'000 with LCS.

The simulations with FLUKA were made separately for several slab thicknesses from 10 cm to 600 cm. The LCS simulations were carried out for slab thicknesses from 2 cm to 180 cm for the iron target. No calculations were made with LCS for the tissue target. The transmission curves at four angles (forward, intermediate, lateral and backward) are shown in Figs. 15-20 for 100, 200 and 400 MeV protons on iron and tissue.

**Shielding parameters**

The contributions to the total dose equivalent come mainly from neutrons, but photons are not negligible and can give a substantial contribution at backward angles at the lowest energies. The proton component has some relevance only at the highest energy (see Table 4 for both contributions). The values of the calculated total dose equivalent were fitted with an exponential function:

$$H(E_p,\theta,d/\lambda_\theta)=\frac{H_0(E_p,\theta)}{r^2}\exp\left[-\frac{d}{\lambda_\theta\cos\theta}\right]$$

in which $H$ is the dose equivalent beyond the shield, $H_0$ is the source term along the direction $\theta$ with respect to the beam, $r$ is the distance between the radiation source (the target stopping the protons) and the point where the dose equivalent is scored, $d$ is the shielding thickness and $\lambda_\theta$ is the attenuation length in the material in the direction $\theta$.

**Table 4** Percentage contributions to total dose equivalent due to proton and photon for iron and tissue targets bombarded by 100, 150, 200, 250, 400 MeV protons.

| Fe | | | | | | | | |
|---|---|---|---|---|---|---|---|---|
| $E_p$ (MeV) | 0°-10° | | 40°-50° | | 80°-90° | | 140°-150° | |
| | $H_\gamma/H_{tot}$ | $H_p/H_{tot}$ | $H_\gamma/H_{tot}$ | $H_p/H_{tot}$ | $H_\gamma/H_{tot}$ | $H_p/H_{tot}$ | $H_\gamma/H_{tot}$ | $H_p/H_{tot}$ |
| 100 | 3.0 | — | 6.0 | — | 20.0 | — | 48.0 | — |
| 150 | 1.9 | — | 2.5 | — | 6.8 | — | 30.0 | — |
| 200 | 1.8 | — | 1.9 | — | 5.0 | — | 36.0 | — |
| 250 | 1.9 | — | 1.9 | — | 3.7 | — | 19.0 | — |
| 400 | 1.6 | 10.7 | 1.6 | 7.0 | 1.8 | 4.3 | 2.3 | 3.1 |
| Tissue | | | | | | | | |
| $E_p$ (MeV) | 0°-10° | | 40°-50° | | 80°-90° | | 140°-150° | |
| | $H_\gamma/H_{tot}$ | $H_p/H_{tot}$ | $H_\gamma/H_{tot}$ | $H_p/H_{tot}$ | $H_\gamma/H_{tot}$ | $H_p/H_{tot}$ | $H_\gamma/H_{tot}$ | $H_p/H_{tot}$ |
| 100 | 5.6 | — | 13.6 | — | 33.3 | — | 50.0 | — |
| 150 | 2.1 | — | 2.5 | — | 3.5 | — | 40.0 | — |
| 200 | 1.8 | — | 2.4 | — | 6.9 | — | 20.0 | — |
| 250 | 1.6 | — | 2.0 | — | 4.7 | — | 10.0 | — |
| 400 | 1.6 | 9.9 | 1.7 | 7.5 | 1.8 | 4.5 | 6.0 | 3.5 |

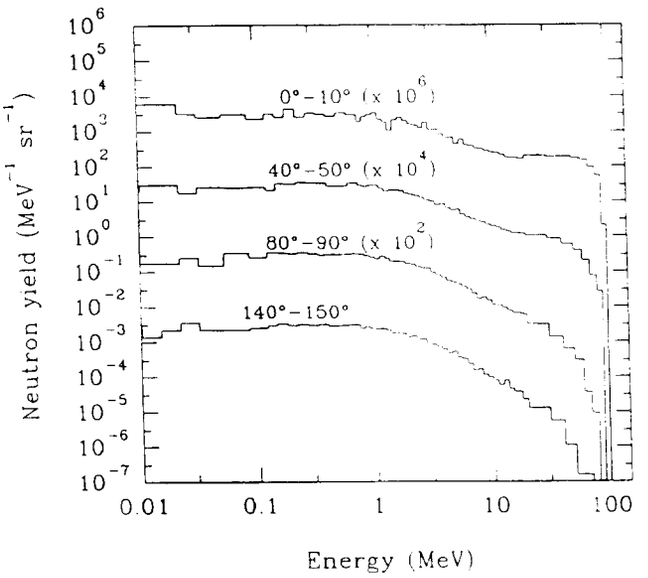


Fig. 4 Double differential neutron distributions per proton for 100 MeV protons striking a thick iron target.

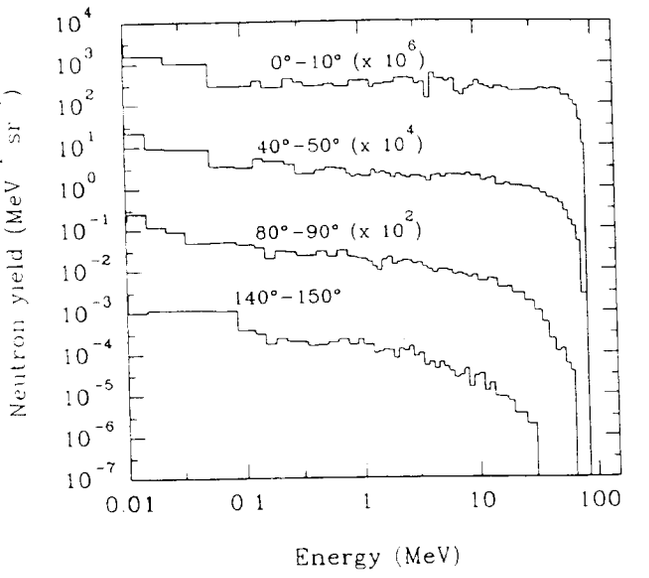


Fig. 5 Double differential neutron distributions per proton for 100 MeV protons striking a thick tissue target.

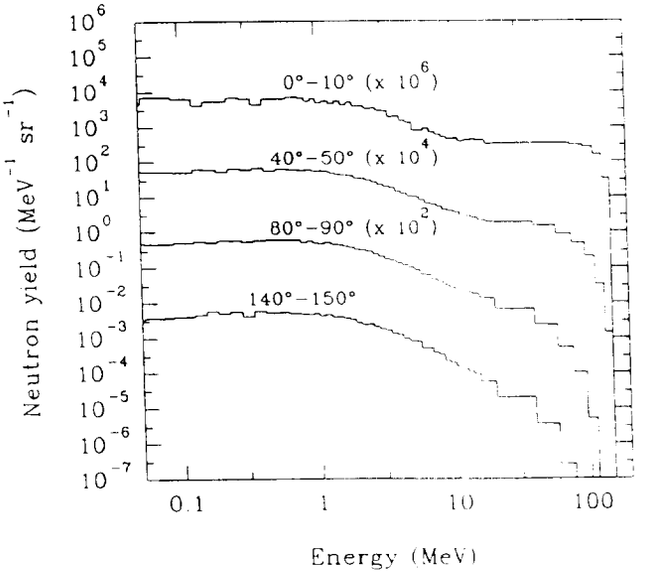


Fig. 6 Double differential neutron distributions per proton for 150 MeV protons striking a thick iron target.

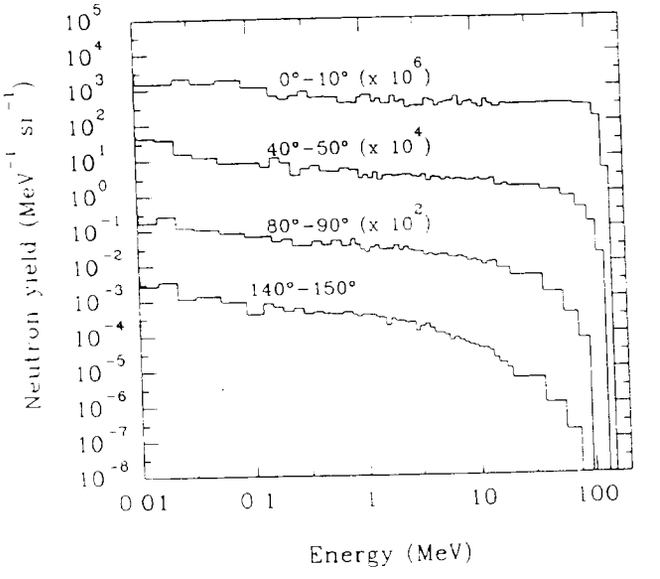


Fig. 7 Double differential neutron distributions per proton for 150 MeV protons striking a thick tissue target.

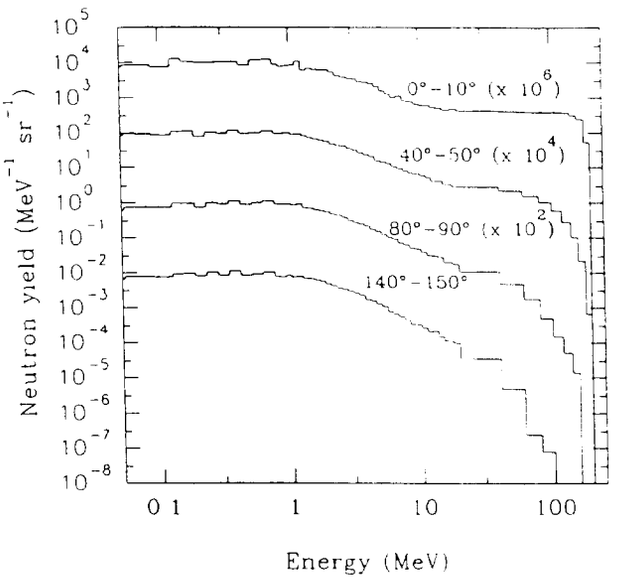


Fig. 8 Double differential neutron distributions per proton for 200 MeV protons striking a thick iron target.

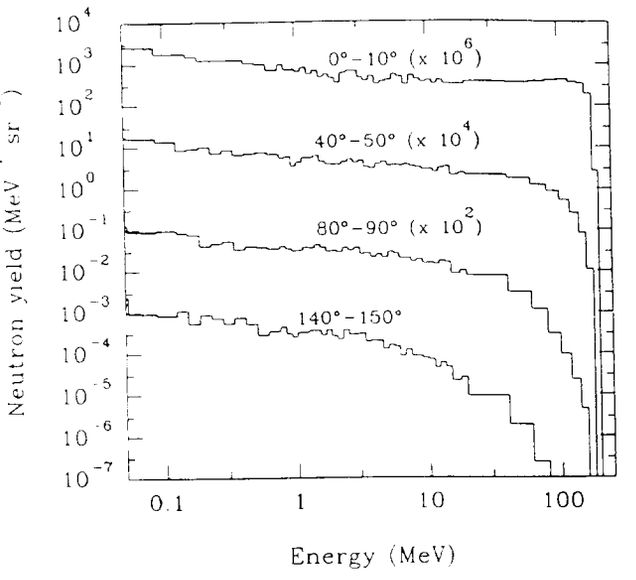


Fig. 9 Double differential neutron distributions per proton for 200 MeV protons striking a thick tissue target.

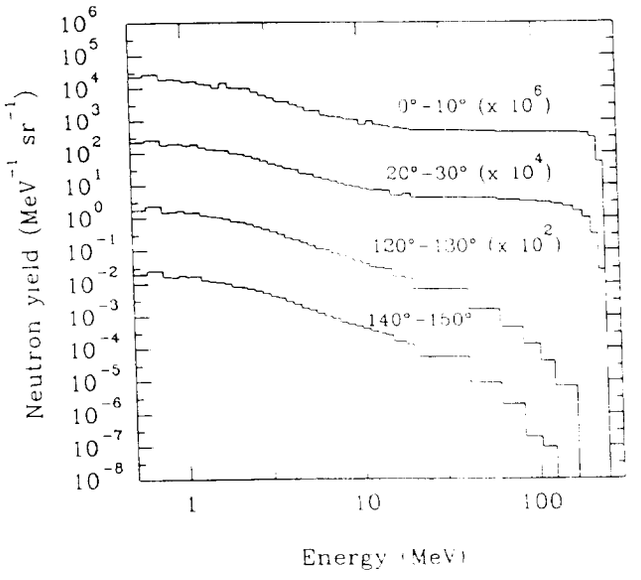


Fig. 10 Double differential neutron distributions per proton for 250 MeV protons striking a thick iron target.

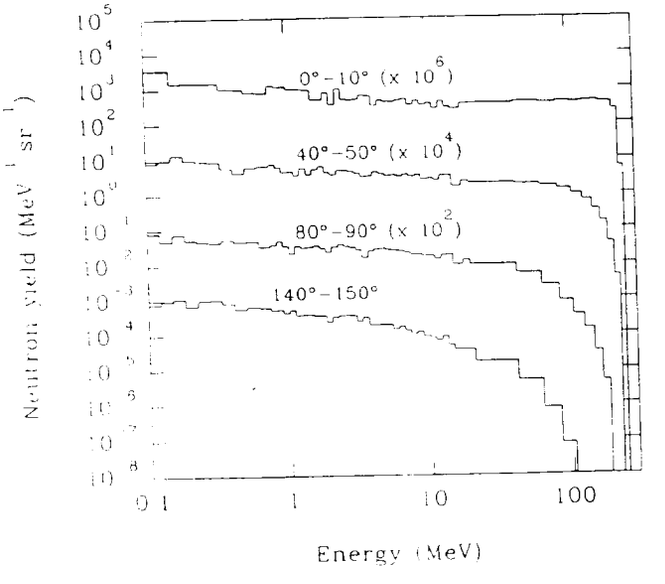


Fig. 11 Double differential neutron distributions per proton for 250 MeV protons striking a thick tissue target.

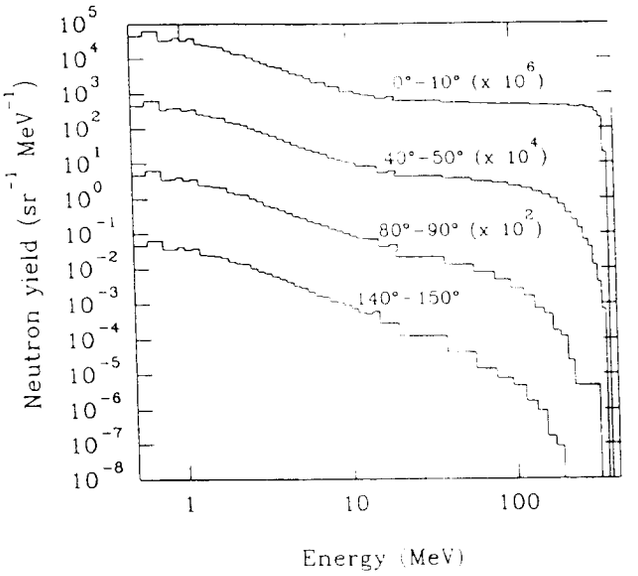


Fig. 12 Double differential neutron distributions per proton for 400 MeV protons striking a thick iron target.

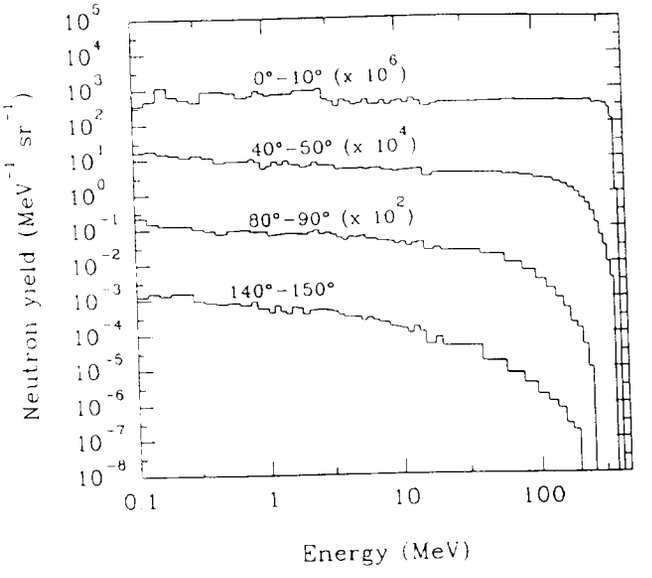


Fig. 13 Double differential neutron distributions per proton for 400 MeV protons striking a thick tissue target.

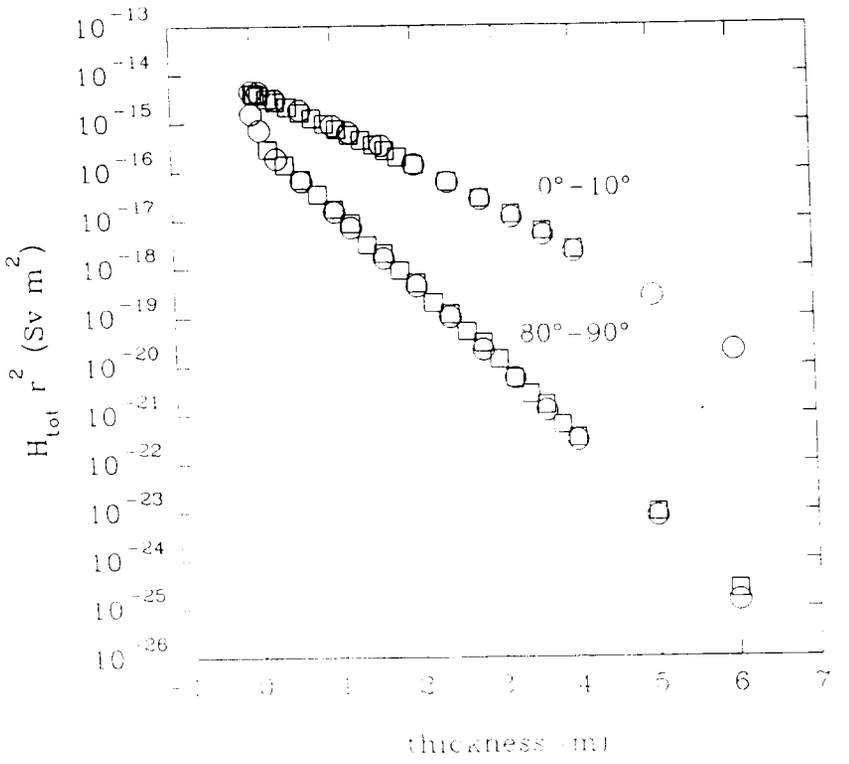


Fig. 14 Comparison between results per proton in slab geometry (squares) and spherical geometry (circles) for 250 MeV protons striking a thick iron target.

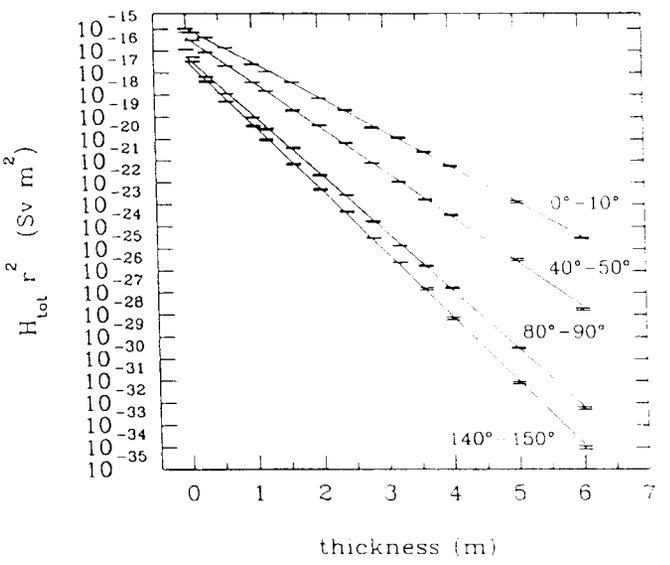


Fig. 15 Total dose equivalent attenuation per proton in ordinary concrete for 100 MeV protons striking a thick iron target.

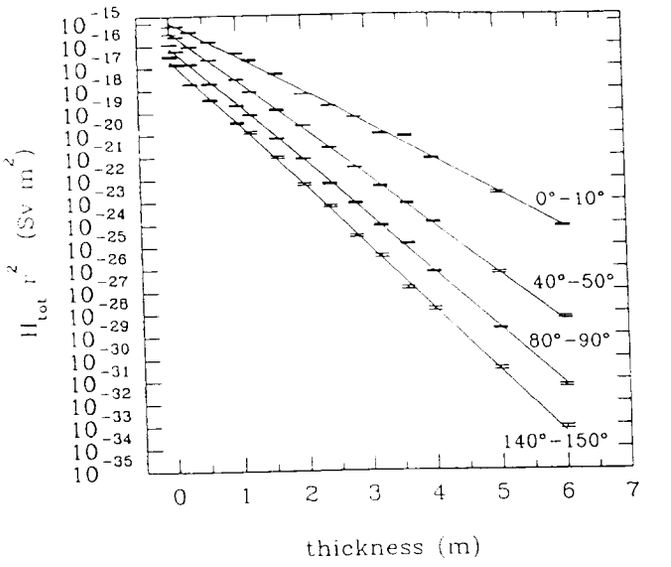


Fig. 16 Total dose equivalent attenuation per proton in ordinary concrete for 100 MeV protons striking a thick tissue target.

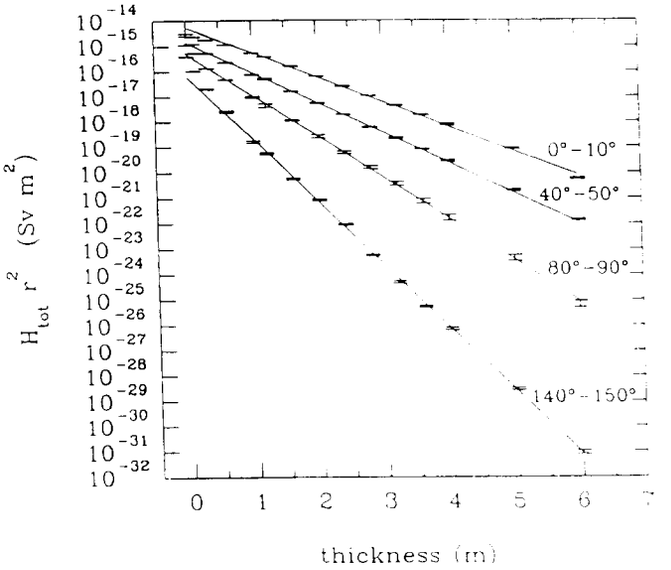


Fig. 17 Total dose equivalent attenuation per proton in ordinary concrete for 200 MeV protons striking a thick iron target.

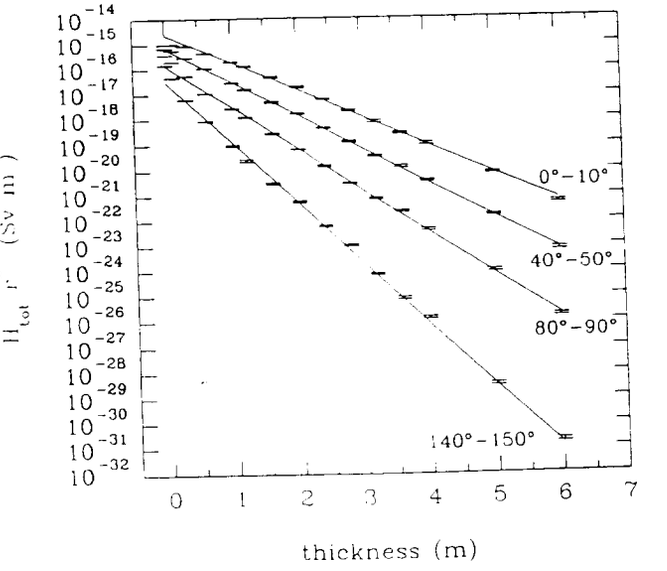


Fig. 18 Total dose equivalent attenuation per proton in ordinary concrete for 200 MeV protons striking a thick tissue target.

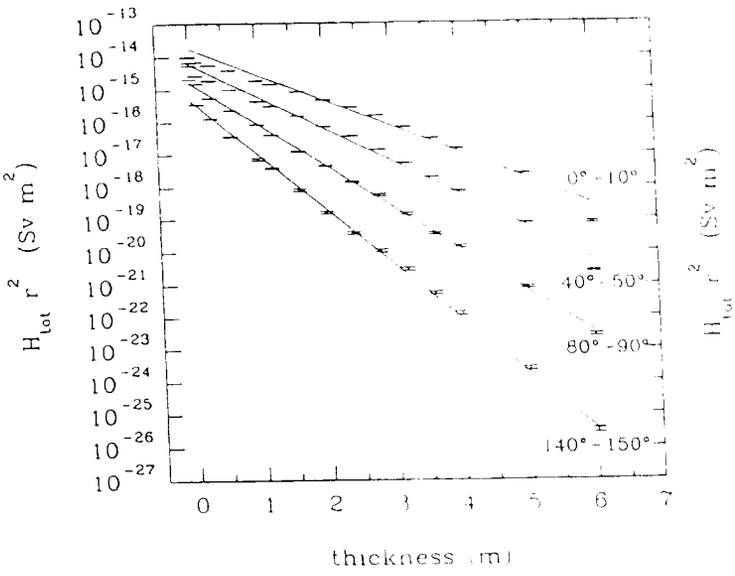


Fig. 19 Total dose equivalent attenuation per proton in ordinary concrete for 400 MeV protons striking a thick iron target.

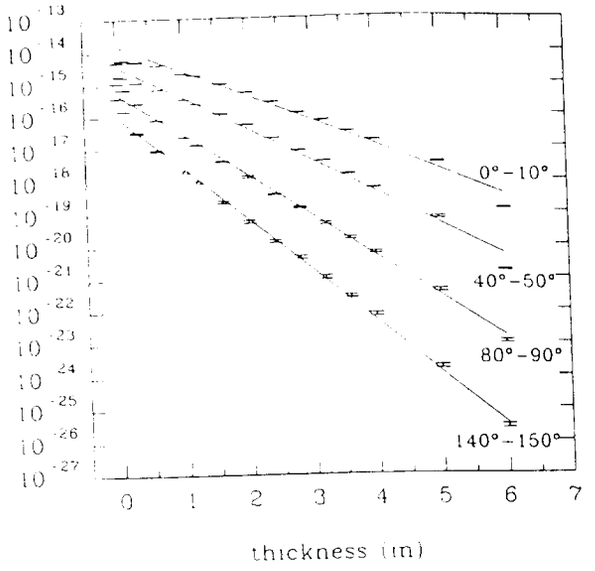


Fig. 20 Total dose equivalent attenuation per proton in ordinary concrete for 400 MeV protons striking a thick tissue target.

The source terms per proton $H_0$ (Sv m$^2$) and the attenuation lengths $\lambda$ (g cm$^{-2}$) are given in the Appendix for the various energies and targets. The deviations of the Monte Carlo data from the best fit are within 15 % in all cases. Here $\lambda$ has been obtained by fitting the data for concrete thicknesses above a certain value (0.5 m at 100 MeV to larger than 2 m at 400 MeV), where the attenuation is roughly exponential. For lower shielding thickness the transmission curve is no longer strictly exponential. This is because the neutron spectrum has not reached equilibrium in the material. Including data at lower thicknesses in the fit, results in an overestimate of $\lambda$ and an underestimate of $H_0$. The estimated attenuation length decreases with increasing the minimum shielding thickness included in the fit and reaches a value approximately constant only at a depth in the material which depends on the incoming proton energy. This behaviour for the iron target is shown in Fig. 21 two proton energies (200 and 400 MeV), where the present results are also compared with those from ref. [17]. Fig. 22 shows the same for the tissue target. Figs. 23 and 24 show, for three energies and the iron target, the behaviour of $H_0$ and $\lambda$ as a function of angle $\theta$. The "jump" observed in the source term at 100 MeV and 200 MeV (Fig. 23) is related to the variation in the attenuation length at the corresponding angles. Figs. 25 and 26 show $H_0$ and $\lambda$ versus proton energy at forward, lateral and backward angles $\theta$, for the iron target. Figs. 27-30 show the same quantities for the tissue target.

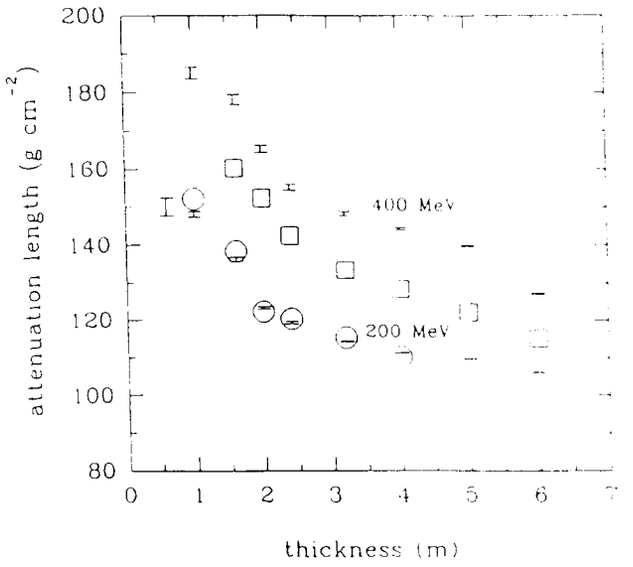


Fig. 21 Attenuation length versus concrete thickness for 200 and 400 MeV protons striking a thick iron target at 0°-10°. Circles and squares are data from ref. [17] at 200 and 400 MeV respectively.

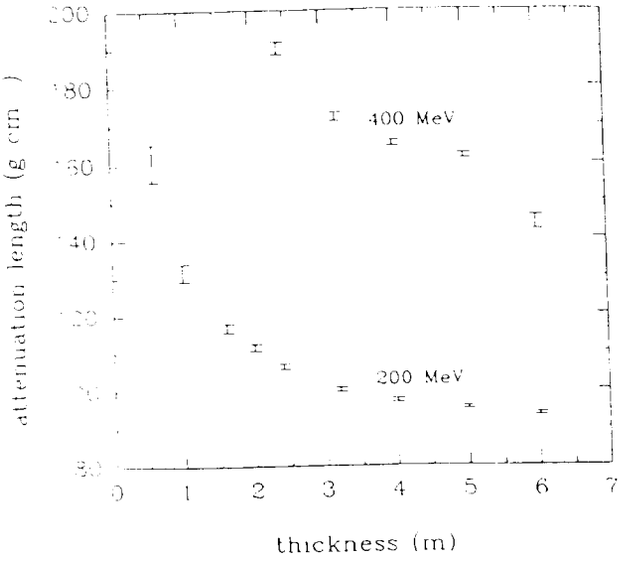


Fig. 22 Attenuation length versus concrete thickness for 200 and 400 MeV protons striking a thick tissue target at 0°-10°.

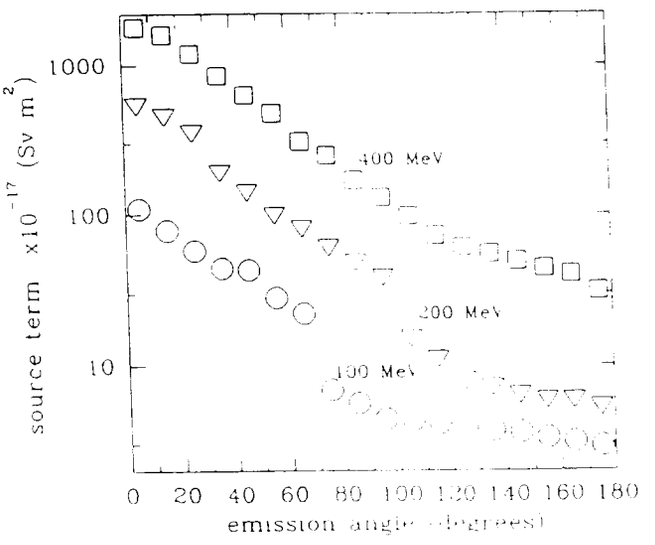


Fig. 23 Source term per proton versus emission angle for 100, 200 and 400 MeV protons striking a thick iron target.

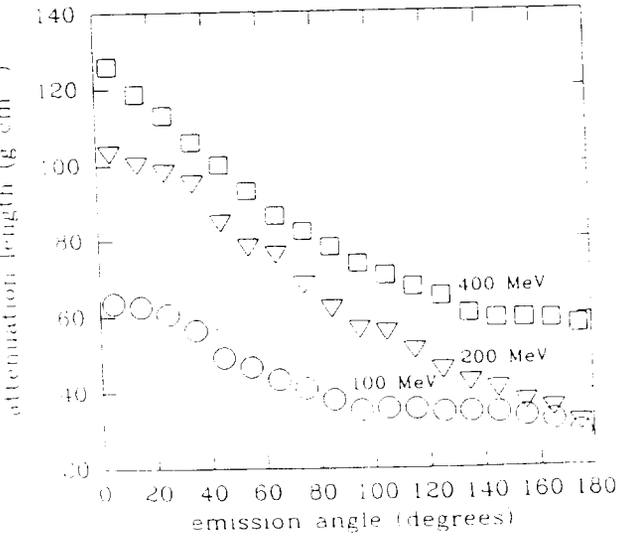


Fig. 24 Attenuation length versus emission angle for 100, 200 and 400 MeV protons striking a thick iron target.

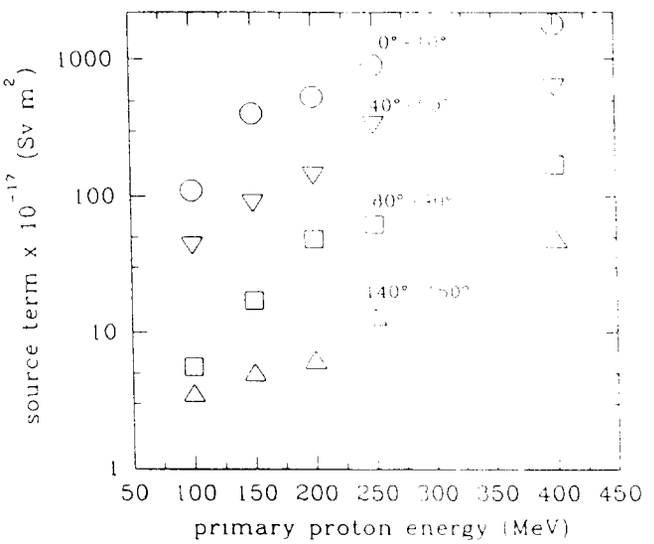


Fig. 25 Source term per proton versus primary proton energy at 0°-10°, 40°-50°, 80°-90° and 140°-150° for a thick iron target.

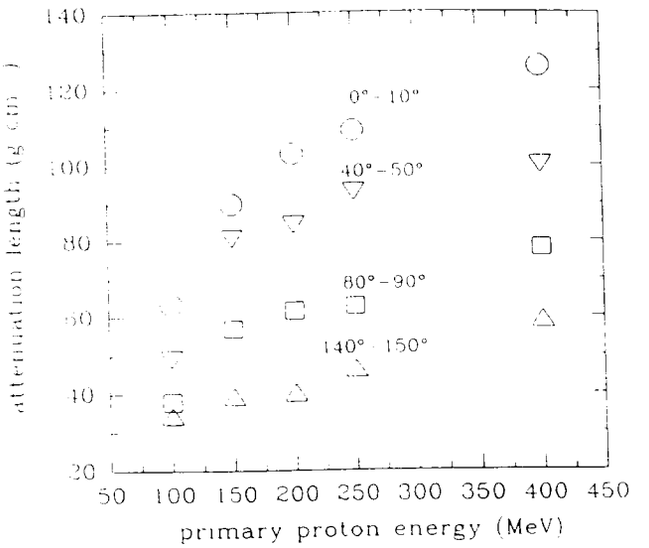


Fig. 26 Attenuation length versus primary proton energy at 0°-10°, 40°-50°, 80°-90° and 140°-150° for a thick iron target.

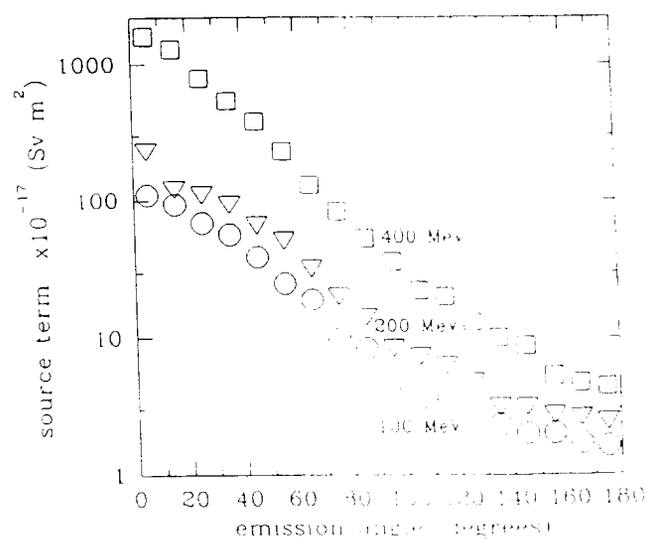


Fig. 27 Source term per proton versus emission angle for 100, 200 and 400 MeV protons striking a thick tissue target.

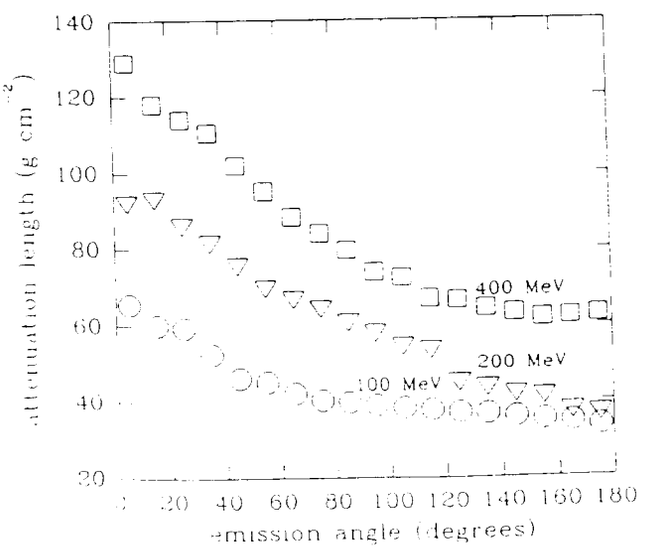


Fig. 28 Attenuation length versus emission angle for 100, 200 and 400 MeV protons striking a thick tissue target.

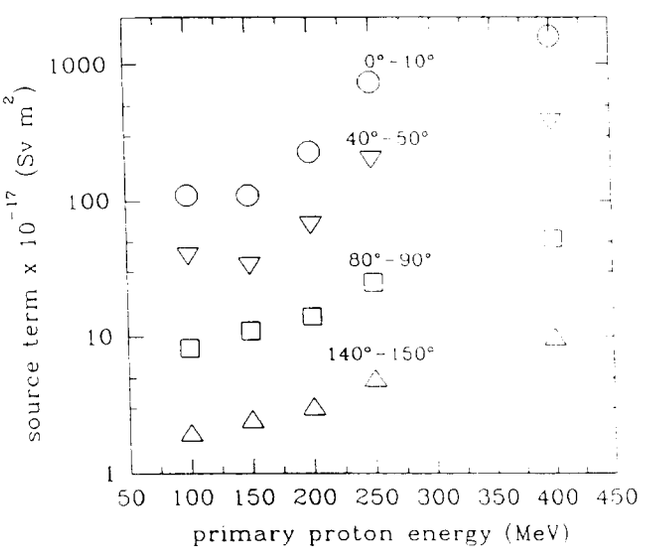


Fig. 29 Source term per proton versus primary proton energy at 0°-10°, 40°-50°, 80°-90° and 140°-150° for a thick tissue target.

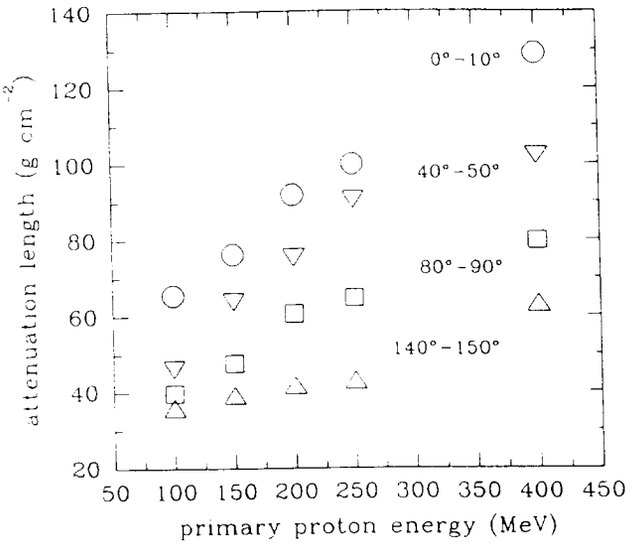


Fig. 30 Attenuation length versus primary proton energy at 0°-10°, 40°-50°, 80°-90° and 140°-150° for a thick tissue target.

The values of $H_0$ and $\lambda$ for the iron target were compared with calculated and experimental data available in the literature [18-24] and listed in Table 5. No literature data are available for a comparison for the tissue target. Data from ref. [18] are results of Monte Carlo calculations with the FLUKA code, for a slightly different type of concrete. The source terms agree within 10% with the values calculated in the present work, while the attenuation lengths are within 6%. Data from ref. [19] are Monte Carlo calculations performed with the High Energy Transport Code (HETC-DO) [25]. The source was placed at the centre of a concrete sphere and scoring was done inside the material. No results are given for the source term. The simulations were done with angular bins larger than those used in the present work (see Table 5). Differences are within 30%. Ref. [20] reports experimental results from measurements with 230 MeV protons, performed at Fermi National Accelerator Laboratory (Batavia, IL) with the proton synchrotron now installed at Loma Linda University Medical Center (California). The concrete composition is substantially different from that employed in the present calculations, which may explain the 20% difference between the attenuation lengths determined experimentally and calculated here. The concrete density is also lower than usual, but this should not affect the comparison. The measurements were carried out inside cavities in the shield and the measured quantity (lineal energy spectrum) differed considerably from the ambient dose equivalent used in the present paper. The agreement between the source terms is good. $H_0$ and $\lambda$ for copper were calculated in ref. [21] by applying empirical correction factors to the values obtained for an aluminum target. The data are given in angular bins larger than those used in the present work. Differences for both source terms and attenuation lengths are within 15%. Data from ref. [22] are LCS results. Differences in the attenuation lengths are within 15%, while the source term calculated in the present work is higher by 17% at 0° and lower by 38% at 90°. Data from ref. [23] are analytical calculations for forward emission only. A comparison with the present results shows a discrepancy for source terms within 30% and within 20% for the attenuation lengths. Finally, ref. [24] reports data for lateral shielding obtained by fitting data from the literature. According to the energy, the agreement with the present results is within 25% for the attenuation length. For the

source term there is a discrepancy of a factor 2 at 400 MeV, while the agreement at the other energies is good. From the above discussion it can be concluded that the agreement between the present calculations and the literature data summarised in Table 5 is in general satisfactory.

**Table 5** Literature data for source term per proton and attenuation length in concrete for forward and lateral shielding for neutrons produced by 100 - 400 MeV protons on copper and iron targets. Literature data from refs. 19-24 refer to neutron attenuation only.

| Author | $E_p$ (MeV) | | Target | | Emission angle | | $\lambda$ (g cm$^{-2}$) | | $H_0$ (Sv m$^2$) | |
|---|---|---|---|---|---|---|---|---|---|---|
| | lit. data | pres. work | lit. data | pres. work | literature data | present work | literature data | present work | literature data | present work |
| Fassò et al. [18] | 100 | 100 | Cu | Fe | 0°-5° | 0°-10° | 60 | 63.6 | 9.1E-16 | 1.1E-15 |
| | 250 | 250 | Cu | Fe | 0°-5° | 0°-10° | 111 | 109 | 9.6E-15 | 9.0E-15 |
| | | | | | 20°-30° | 20°-30° | 114 | 110 | 4.5E-15 | 6.8E-15 |
| Hagan et al. [19] | 250 | 250 | Fe | Fe | 0°-15° | 0°-10° | 109 | 109 | | |
| | | | | | 15°-30° | 20°-30° | 105 | 110 | | |
| | | | | | 30°-45° | 40°-50° | 93 | 92.9 | | |
| | | | | | 45°-60° | 50°-60° | 99 | 89 | | |
| | | | | | 60°-90° | 80°-90° | 88 | 62.8 | | |
| Siebers et al. [20] | 230 | 250 | Fe | Fe | 0° | 0°-10° | 90 | 109 | 7.9E-15 | 9.0E-15 |
| | | | | | 22° | 20°-30° | 88 | 110 | 4.7E-15 | 6.8E-15 |
| | | | | | 45° | 40°-50° | 75 | 92.9 | 2.7E-15 | 3.3E-15 |
| | | | | | 90° | 80°-90° | 51.9 | 62.8 | 7.6E-16 | 6.2E-16 |
| Awschalom [21] | 250 | 250 | Cu | Fe | 0°-30° | 0°-10° | 104 | 109 | 5.6E-15 | 9.0E-15 |
| | | | | | 30°-60° | 50°-60° | 93 | 89 | 2.2E-15 | 2.5E-15 |
| | | | | | 60°-90° | 80°-90° | 73 | 62.8 | 4.1E-16 | 6.2E-16 |
| Knowles et al. [22] | 230 | 250 | Fe | Fe | 0°-10° | 0°-10° | 99 | 109 | 6.6E-15 | 9.0E-15 |
| | | | | | 10°-30° | 20°-30° | 104 | 110 | 5.0E-15 | 7.5E-15 |
| | | | | | 40°-50° | 40°-50° | 89.4 | 92.9 | 2.3E-15 | 3.3E-15 |
| | | | | | 85°-95° | 80°-90° | 53.4 | 62.8 | 1.0E-15 | 6.2E-16 |
| Braid et al. [23] | 100 | 100 | Cu | Fe | 0° | 0°-10° | 77 | 63.6 | 1.8E-15 | 1.1E-15 |
| | 200 | 200 | Cu | Fe | 0° | 0°-10° | 90 | 103 | 7.4E-15 | 5.3E-15 |
| | 400 | 400 | Cu | Fe | 0° | 0°-10° | 127 | 126 | 1.3E-14 | 1.8E-14 |
| Tesch et al. [24] | 100 | 100 | Fe | Fe | 90° | 80°-90° | 50 | 38 | 4.0E-17 | 5.6E-17 |
| | 250 | 250 | Fe | Fe | 90° | 80°-90° | 78 | 62.8 | 6.0E-16 | 6.2E-16 |
| | 400 | 400 | Fe | Fe | 90° | 80°-90° | 89 | 78.1 | 3.2E-15 | 1.7E-15 |

## Conclusions

This paper provides complete information for shielding calculations of proton accelerators in the energy range 100-400 MeV and compares the energy and angular distributions generated by the Monte Carlo codes FLUKA and LCS. The two codes give similar results concerning the neutron emission from the target, although LCS gives lower yields at large angles because the pre-equilibrium model is lacking in the version used. For the shielding calculations, the results of the two codes agree at small attenuation depths. At large depths - required in most actual situations - the use of LCS becomes impractical due to the very long computing time required to achieve a sufficient statistics. At the lower end of the energy range considered here, the photon component appears to contribute up to 50 % (for

the backward angles) of the total dose equivalent and cannot be completely neglected in shielding assessments. The photon component may vary with different concrete composition. Secondary protons only give a substantial contribution at the highest energy.

An extensive comparison of source terms and attenuation lengths obtained in the present work with published data shows an acceptable agreement, despite the large differences in the configurations and techniques used. However, literature data are sparse and specific to given beam conditions and geometries. In the present paper an effort has been made to obtain a complete set of parameters which can be used in shielding design of proton facilities of widely different characteristics. These shielding data should to a large extent limit to a minimum the need for long and complex Monte Carlo calculations. The smooth behaviour of $\lambda$ and $H_0$ versus proton energy and polar angle allows to interpolate the present data for application for any energy in the range considered.

## References


1. T. Nakamura, Proc. of the AEN/NEA Specialists' Meeting on Shielding Aspects of Accelerators, Targets and Irradiation Facilities, Arlington (Texas), 28-29 April 1994, NEA/OECD (1995) p. 21
2. T.A. Gabriel, Proc. of the AEN/NEA Specialists' Meeting on Shielding Aspects of Accelerators, Targets and Irradiation Facilities, Arlington (Texas), 28-29 April 1994, NEA/OECD (1995), p. 41
3. M. Silari, Proc. of the AEN/NEA Specialists' Meeting on Shielding Aspects of Accelerators, Targets and Irradiation Facilities, Arlington (Texas), 28-29 April 1994, NEA/OECD (1995), p. 61
4. S. Serezhnikov, I. Azhgirey, A. Uzunian and V. Bamblesky, Proc. of the AEN/NEA Specialists' Meeting on Shielding Aspects of Accelerators, Targets and Irradiation Facilities, Arlington (Texas), 28-29 April 1994, NEA/OECD (1995), p. 81
5. R.H. Thomas and G.R. Stevenson, "Radiological safety aspects of the operation of proton accelerators", Technical report series No. 283, IAEA, Vienna (1988)
6. S. Agosteo, M. G. Corrado, M. Silari and P. Tabarelli de Fatis, "Shielding design for a proton medical accelerator facility", IEEE Trans. Nucl. Sci., in press
7. R.E. Prael and H. Lichtenstein, Radiation Transport Group, Los Alamos National Laboratory (1989)
8. A. Fassò, A. Ferrari, J. Ranft and P.R. Sala, Proc. of the AEN/NEA Specialists' Meeting on Shielding Aspects of Accelerators, Targets and Irradiation Facilities, Arlington (Texas), 28-29 April 1994, NEA/OECD (1995), p. 287
9. International Commission on Radiation Units and Measurements, Report No. 33 Bethesda, Maryland, U.S.A. (1980) p. 20
10. M.M. Meier, C.A. Goulding, G.L. Morgan and J.L. Ullmann, Nucl. Sci. Eng. 104 (1990) 339
11. R.E. Prael, LA-UR-90-1620, Los Alamos National Laboratory, Los Alamos (1990)
12. International Commission on Radiation Units and Measurements, Report No. 49, Bethesda, Maryland, U.S.A. (1993)
13. E.A. Belogorlov et al., Nucl. Instr. and Meth. 199 (1982) 563
14. A.V. Sannikov and E.N. Savitskaya, CERN /TIS-RP/93-14 (1993)
15. International Commission on Radiological Protection, ICRP Publication 21, Pergamon Press (1971)
16. A. Ferrari and M. Pelliccioni, Rad. Prot. Dosim. 51 (1994) 251
17. K. Shin, Comments on "Neutron Attenuation Length and Build-up Factors in Energy Range < 500 MeV", presented at the AEN/NEA Specialists Meeting on Shielding Aspects of Accelerators, Arlington, Texas, USA, April 28-29, 1994
18. A. Fassò, A. Ferrari and G.R. Stevenson, Proc. of the AEN/NEA Specialists' Meeting on Shielding Aspects of Accelerators, Targets and Irradiation Facilities, Arlington (Texas), 28-29 April 1994, NEA/OECD (1995), p. 155
19. N.K. Hagan, B.L. Colborn and T.W. Armstrong Allen, Nucl. Sci. Eng. 98 (1988) 272
20. J.V. Siebers, P.M. DeLuca, D.W. Pearson and G. Coutrakon, Nucl. Sci. Eng. 115 (1993) 13
21. M. Awschalom, FNAL-TM-1354 (1987)
22. H.B. Knowles, J.L. Orthel and B.W. Hill, Proc. of the 1993 Particle Accelerator Conference, Washington D. C., May 17-20, 1993, IEEE (1993), p. 1762
23. T.H. Braid, R.F. Rapids, R.H. Siemssen, J.W. Tippie and K. O'Brien, IEEE Trans. Nucl. Sci. NS-18 (1971) 821
24. K. Tesch, Radiat. Prot. Dosim. 11 (1985) 165
25. T.W. Armstrong and C. Chandler, Nucl. Sci. Eng. 49 (1972) 110

## Appendix

**Table A1** Source term per proton and attenuation length in concrete TSF-5.5 for total dose equivalent from iron and tissue targets bombarded by 100 MeV protons.

| | Fe | | Tissue | |
|---|---|---|---|---|
| Angular bin | $H_0$ (Sv m$^2$) | $\lambda$ (g cm$^{-2}$) | $H_0$ (Sv m$^2$) | $\lambda$ (g cm$^{-2}$) |
| 0°-10° | 1.1E-15 | 63.6 | 1.1E-15 | 65.5 |
| 10°-20° | 7.9E-16 | 62.6 | 9.3E-16 | 60.0 |
| 20°-30° | 5.8E-16 | 60.6 | 6.9E-16 | 59.4 |
| 30°-40° | 4.4E-16 | 56.5 | 5.7E-16 | 52.4 |
| 40°-50° | 4.3E-16 | 49.1 | 3.9E-16 | 46.2 |
| 50°-60° | 2.8E-16 | 46.7 | 2.5E-16 | 45.1 |
| 60°-70° | 2.2E-16 | 43.4 | 1.9E-16 | 42.1 |
| 70°-80° | 6.9E-17 | 41.0 | 9.7E-17 | 40.4 |
| 80°-90° | 5.6E-17 | 38.0 | 8.3E-17 | 39.8 |
| 90°-100° | 4.4E-17 | 35.2 | 4.9E-17 | 39.0 |
| 100°-110° | 4.3E-17 | 35.6 | 3.6E-17 | 38.4 |
| 110°-120° | 4.1E-17 | 35.5 | 3.5E-17 | 37.8 |
| 120°-130° | 3.9E-17 | 34.7 | 3.0E-17 | 37.2 |
| 130°-140° | 3.7E-17 | 34.6 | 2.3E-17 | 36.8 |
| 140°-150° | 3.6E-17 | 34.4 | 2.0E-17 | 36.0 |
| 150°-160° | 3.3E-17 | 33.4 | 2.0E-17 | 35.2 |
| 160°-170° | 3.1E-17 | 32.2 | 1.7E-17 | 34.6 |
| 170°-180° | 2.9E-17 | 29.0 | 1.6E-17 | 33.5 |

**Table A2** Source term per proton and attenuation length in concrete TSF-5.5 for total dose equivalent from iron and tissue targets bombarded by 150 MeV protons.

| | Fe | | Tissue | |
|---|---|---|---|---|
| Angular bin | $H_0$ (Sv m$^2$) | $\lambda$ (g cm$^{-2}$) | $H_0$ (Sv m$^2$) | $\lambda$ (g cm$^{-2}$) |
| 0°-10° | 4.0E-15 | 89.9 | 1.1E-15 | 76.3 |
| 10°-20° | 2.9E-15 | 87.7 | 9.8E-16 | 74.0 |
| 20°-30° | 2.2E-15 | 89.5 | 6.9E-16 | 70.7 |
| 30°-40° | 1.4E-15 | 84.1 | 4.2E-16 | 68.5 |
| 40°-50° | 8.8E-16 | 80.8 | 3.3E-16 | 63.9 |
| 50°-60° | 6.6E-16 | 73.4 | 2.0E-16 | 65.2 |
| 60°-70° | 4.4E-16 | 68.0 | 1.9E-16 | 57.4 |
| 70°-80° | 3.5E-16 | 62.8 | 1.2E-16 | 53.9 |
| 80°-90° | 1.7E-16 | 57.0 | 1.1E-16 | 47.6 |
| 90°-100° | 1.2E-16 | 51.5 | 8.1E-17 | 49.0 |
| 100°-110° | 1.0E-16 | 48.0 | 5.9E-17 | 43.4 |
| 110°-120° | 9.1E-16 | 46.6 | 5.1E-17 | 47.0 |
| 120°-130° | 8.1E-17 | 45.8 | 3.3E-17 | 42.5 |
| 130°-140° | 6.1E-17 | 41.9 | 2.7E-17 | 41.9 |
| 140°-150° | 5.1E-17 | 39.4 | 2.5E-17 | 39.2 |
| 150°-160° | 5.1E-17 | 36.4 | 2.2E-17 | 38.6 |
| 160°-170° | 4.5E-17 | 34.5 | 2.1E-17 | 35.7 |
| 170°-180° | 4.0E-17 | 30.3 | 1.7E-17 | 36.8 |

**Table A3** Source term per proton and attenuation length in concrete TSF-5.5 for total dose equivalent from iron and tissue targets bombarded by 200 MeV protons.

| | Fe | | Tissue | |
|---|---|---|---|---|
| Angular bin | $H_0$ (Sv m$^2$) | $\lambda$ (g cm$^{-2}$) | $H_0$ (Sv m$^2$) | $\lambda$ (g cm$^{-2}$) |
| 0°-10° | 5.3E-15 | 103.0 | 2.3E-15 | 92.0 |
| 10°-20° | 4.5E-15 | 100.0 | 1.2E-15 | 93.0 |
| 20°-30° | 3.5E-15 | 98.0 | 1.1E-15 | 86.0 |
| 30°-40° | 1.9E-15 | 95.0 | 9.3E-16 | 81.5 |
| 40°-50° | 1.4E-15 | 84.5 | 6.6E-16 | 75.5 |
| 50°-60° | 9.8E-16 | 78.0 | 5.1E-16 | 69.6 |
| 60°-70° | 8.0E-16 | 76.0 | 3.2E-16 | 66.7 |
| 70°-80° | 6.0E-16 | 68.0 | 2.0E-16 | 64.3 |
| 80°-90° | 4.8E-16 | 61.8 | 1.4E-16 | 60.7 |
| 90°-100° | 3.8E-16 | 56.3 | 8.3E-17 | 57.9 |
| 100°-110° | 1.5E-16 | 55.5 | 7.2E-17 | 54.4 |
| 110°-120° | 1.1E-16 | 50.7 | 6.2E-17 | 53.4 |
| 120°-130° | 7.9E-17 | 45.5 | 4.7E-17 | 44.8 |
| 130°-140° | 7.1E-17 | 42.2 | 3.1E-17 | 43.5 |
| 140°-150° | 6.3E-17 | 40.3 | 3.1E-17 | 41.7 |
| 150°-160° | 5.8E-17 | 36.9 | 2.7E-17 | 41.1 |
| 160°-170° | 5.8E-17 | 35.1 | 2.6E-17 | 37.2 |
| 170°-180° | 5.2E-17 | 31.1 | 2.4E-17 | 36.5 |

**Table A4** Source term per proton and attenuation length in concrete TSF-5.5 for total dose equivalent from iron and tissue targets bombarded by 250 MeV protons.

| | Fe | | Tissue | |
|---|---|---|---|---|
| Angular bin | $H_0$ (Sv m$^2$) | $\lambda$ (g cm$^{-2}$) | $H_0$ (Sv m$^2$) | $\lambda$ (g cm$^{-2}$) |
| 0°-10° | 9.0E-15 | 109.0 | 7.4E-15 | 100.0 |
| 10°-20° | 7.5E-15 | 106.0 | 5.4E-15 | 101.0 |
| 20°-30° | 6.8E-15 | 110.0 | 3.5E-15 | 96.7 |
| 30°-40° | 3.9E-15 | 98.7 | 3.3E-15 | 90.5 |
| 40°-50° | 3.3E-15 | 92.9 | 2.0E-15 | 84.5 |
| 50°-60° | 2.5E-15 | 89.0 | 1.2E-15 | 79.8 |
| 60°-70° | 2.0E-15 | 83.7 | 7.1E-16 | 76.7 |
| 70°-80° | 8.1E-16 | 78.2 | 4.1E-16 | 68.9 |
| 80°-90° | 6.2E-16 | 62.8 | 2.5E-16 | 61.8 |
| 90°-100° | 3.8E-16 | 60.1 | 1.6E-16 | 56.5 |
| 100°-110° | 2.9E-16 | 54.9 | 9.3E-17 | 56.8 |
| 110°-120° | 1.9E-16 | 55.9 | 8.1E-17 | 52.4 |
| 120°-130° | 1.6E-16 | 52.8 | 7.5E-17 | 51.9 |
| 130°-140° | 1.5E-16 | 45.9 | 6.2E-17 | 50.5 |
| 140°-150° | 1.3E-16 | 46.4 | 5.0E-17 | 43.0 |
| 150°-160° | 9.4E-17 | 37.5 | 4.6E-17 | 42.3 |
| 160°-170° | 8.0E-17 | 37.3 | 3.4E-17 | 40.9 |
| 170°-180° | 6.5E-17 | 32.8 | 3.0E-17 | 38.0 |

**Table A5** Source term per proton and attenuation length in concrete TSF-5.5 for total dose equivalent from iron and tissue targets bombarded by 400 MeV protons.

| | Fe | | Tissue | |
|---|---|---|---|---|
| Angular bin | $H_0$ (Sv m$^2$) | $\lambda$ (g cm$^{-2}$) | $H_0$ (Sv m$^2$) | $\lambda$ (g cm$^{-2}$) |
| 0°-10° | 1.8E-14 | 126.0 | 1.6E-14 | 129.0 |
| 10°-20° | 1.6E-14 | 118.7 | 1.3E-14 | 118.0 |
| 20°-30° | 1.2E-14 | 113.0 | 7.9E-15 | 114.0 |
| 30°-40° | 8.5E-15 | 106.0 | 5.4E-15 | 110.5 |
| 40°-50° | 6.3E-15 | 99.9 | 3.8E-15 | 102.0 |
| 50°-60° | 4.8E-15 | 93.0 | 2.3E-15 | 95.3 |
| 60°-70° | 3.1E-15 | 86.4 | 1.3E-15 | 88.4 |
| 70°-80° | 2.5E-15 | 82.2 | 8.3E-16 | 84.1 |
| 80°-90° | 1.7E-15 | 78.1 | 5.3E-16 | 79.7 |
| 90°-100° | 1.3E-15 | 73.6 | 3.6E-16 | 74.0 |
| 100°-110° | 9.8E-16 | 70.5 | 2.2E-16 | 72.6 |
| 110°-120° | 7.3E-16 | 67.6 | 2.0E-16 | 67.1 |
| 120°-130° | 6.1E-16 | 65.1 | 1.3E-16 | 66.6 |
| 130°-140° | 5.5E-16 | 60.5 | 1.0E-16 | 64.5 |
| 140°-150° | 4.9E-16 | 59.1 | 1.0E-16 | 63.2 |
| 150°-160° | 4.4E-16 | 59.1 | 5.3E-17 | 61.9 |
| 160°-170° | 4.0E-16 | 58.8 | 4.7E-17 | 62.3 |
| 170°-180° | 3.1E-16 | 57.3 | 4.4E-17 | 62.8 |